Arctic and Tibetan Plateau Tundra Show Divergent Temperature and Precipitation Thresholds Under Climate Change

Citation for the original published paper (version of record):

Zhu, H., Yu, H., Chen, H. et al (2026). Arctic and Tibetan Plateau Tundra Show Divergent Temperature and Precipitation Thresholds Under Climate Change. Geophysical Research Letters, 53(16). http://dx.doi.org/10.1029/2026GL124727

(article starts on next page)

Geophysical Research Letters

RESEARCH LETTER

10.1029/2026GL124727

Arctic and Tibetan Plateau Tundra Show Divergent Temperature and Precipitation Thresholds Under Climate Change

Huajie Zhu[1], **Han Yu**[1], **Hans W. Chen**[2], **Ziqian Zhong**[2], **Wenzhuo Duan**[1], **Songhan Wang**[3], and **Mousong Wu**[1,4]

[1]International Institute for Earth System Science, Nanjing University, Nanjing, China, [2]Department of Environmental and Energy Sciences, Chalmers University of Technology, Gothenburg, Sweden, [3]Jiangsu Collaborative Innovation Center for Modern Crop Production/Key Laboratory of Crop Physiology and Ecology in Southern China, College of Agriculture, Nanjing Agricultural University, Nanjing, China, [4]Frontiers Science Center for Critical Earth Material Cycling, Nanjing University, Nanjing, China

Key Points:

- Arctic and Tibetan Plateau tundra exhibit distinct temperature and precipitation thresholds for gross primary productivity
- Temperature thresholds rise steadily in both regions while precipitation thresholds diverge under future climate change
- By 2100, Arctic browning zones are more precipitation-constrained, whereas greening zones are more temperature-constrained

Supporting Information:

Supporting Information may be found in the online version of this article.

Correspondence to:

H. W. Chen and M. Wu,
hans.chen@chalmers.se;
mousongwu@nju.edu.cn

Citation:

Zhu, H., Yu, H., Chen, H. W., Zhong, Z., Duan, W., Wang, S., & Wu, M. (2026). Arctic and Tibetan Plateau tundra show divergent temperature and precipitation thresholds under climate change. *Geophysical Research Letters*, *53*, e2026GL124727. https://doi.org/10.1029/2026GL124727

Received 1 JUN 2026
Accepted 5 AUG 2026

Author Contributions:

Conceptualization: Mousong Wu
Funding acquisition: Mousong Wu
Methodology: Mousong Wu
Visualization: Wenzhuo Duan
Writing – original draft: Huajie Zhu, Han Yu
Writing – review & editing: Hans W. Chen, Ziqian Zhong, Songhan Wang

Abstract The Arctic and Tibetan Plateau (TP) have experienced pronounced warming and shifts in precipitation patterns, yet vegetation responses to climate change remain insufficiently understood. Here, we analyze the temperature and precipitation thresholds of limiting gross primary productivity (GPP) of tundra ecosystems in the Arctic and TP from 1982 to 2100, using a combination of observational data sets and simulations. We found that the temperature thresholds limiting GPP increase in both regions have steadily increased since 1982 and are projected to continue rising. In contrast, precipitation thresholds show significant upward trends in the Arctic but considerable temporal variability in the TP. By 2100, precipitation limitation of GPP is projected to exert a stronger influence in browning zones than in greening zones, whereas temperature limitation is more pronounced in greening zones. Our results reveal the diverse vegetation responses to temperature and precipitation in the Arctic and TP tundra.

Plain Language Summary Plants absorb carbon dioxide (CO_2) from the atmosphere through photosynthesis, and this capacity is constrained by temperature and precipitation. In recent decades, the Arctic and the Tibetan Plateau have experienced rapid warming and substantial shifts in precipitation patterns. This study investigates how tundra in these regions is affected by temperature and precipitation from 1982 to 2100, using both long-term observations and future climate projections. We found that the temperature level above which photosynthesis is no longer limited by cold has been rising for decades and is expected to keep increasing. However, it will remain higher than the average temperature during the growing season, indicating that temperature will continue to limit plant photosynthesis. For precipitation, tundra in the Arctic will need more precipitation to avoid water stress, while the Tibetan Plateau shows great variability in this precipitation threshold. By the end of the century, water limitation is projected to be more severe in browning areas, while temperature limitation will be more pronounced in greening areas. These findings highlight different climate constraints on Arctic and Tibetan Plateau tundra, with important implications for predicting carbon–climate interactions.

1. Introduction

Over recent decades, both the Arctic and the Tibetan Plateau (TP) have undergone pronounced warming, at rates approximately 2–4 times the global average (Blunden & Arndt, 2020; Rantanen et al., 2022; You et al., 2021). Rising temperatures typically enhance vegetation photosynthetic capacity by accelerating photosynthetic rates and extending the growing season (Goetz et al., 2005; Piao et al., 2020) before reaching a temperature threshold, beyond which vegetation ceases to be temperature-limited and becomes controlled by non-temperature factors (Donohue et al., 2013). Currently, both satellite-based vegetation dynamics monitoring and field surveys indicate increasing photosynthetic productivity in the Arctic and TP (Berner et al., 2020; Epstein et al., 2012; Keenan & Riley, 2018; Zhu et al., 2016). However, it remains unclear how the vegetation temperature thresholds in these regions have evolved over recent decades and how they may respond to future climate change. Understanding these dynamics is critical for improving projections of carbon–climate feedbacks.

In addition to temperature changes, the Arctic and TP have also experienced an overall increase in precipitation in recent decades (Bintanja & Selten, 2014; Wang et al., 2018). Projections indicate that Arctic precipitation may rise by as much as 50% by the end of this century (Kattsov et al., 2007). Across the TP, precipitation trends are spatially heterogeneous, with increases observed across most of the region, particularly in the eastern and central parts (Xu et al., 2008). Increased precipitation generally alleviates vegetation water stress and thereby enhances photosynthetic capacity (Maricle & Adler, 2011); however, this effect may saturate or decline beyond a certain threshold (Huxman et al., 2004; Z. Liu et al., 2018). For example, primary productivity in the United States increases with mean annual precipitation but plateaus at approximately 1,000 mm (Maurer et al., 2020). Nevertheless, precipitation thresholds for vegetation productivity in the Arctic and TP, and their temporal dynamics, remain unclear (Zhong et al., 2010).

Tundra ecosystems, which dominate both the Arctic and TP, experience minimal direct human disturbance and thus serve as sensitive indicators of climate change. The Arctic and TP exhibit distinct local climates shaped by factors including latitude, topography, and regional atmospheric circulation patterns (Margesin, 2008; You et al., 2021). In this context, although tundra ecosystems have shown widespread greening over the past decades, browning has also been evident and displays contrasting characteristics across these two regions (Berner et al., 2020; Li et al., 2020). Given that tundra ecosystems are expected to exert a substantial influence on both the magnitude and rate of global warming (Loranty & Goetz, 2012), it is therefore essential to investigate the photosynthetic responses and projected trajectories of tundra vegetation under climate change, particularly through separate analyses of greening and browning regions.

Here, we integrated observational records and Coupled Model Intercomparison Project Phase 6 (CMIP6) Earth System Model (ESM) simulations of gross primary productivity (GPP), temperature, and precipitation to identify greening and browning zones across the Arctic and TP, and to examine the vegetation temperature and precipitation thresholds limiting tundra GPP from 1982 to 2100. The objectives of this study are to: (a) quantify historical trends (1982–2014) in the GPP-limiting temperature and precipitation thresholds in the Arctic and TP tundra ecosystems; (b) project how these thresholds will change under different Shared Socioeconomic Pathways (SSPs) from 2015 to 2100; and (c) distinguish temperature and precipitation constraints between greening and browning zones in the Arctic and TP.

2. Materials and Methods

2.1. Data

This study focuses on tundra ecosystems in the Eurasian Arctic (EA) and North American Arctic (NA) north of 60°N, and on the Tibetan Plateau (TP) in China (Figure 1a). Tundra was defined as grassland and shrubland within permafrost regions using the 2018 Moderate Resolution Imaging Spectroradiometer (MODIS) land-cover product based on the International Geosphere–Biosphere Program (IGBP) classification scheme (Epstein et al., 2012; Xu et al., 2013). The 2018 land-cover data set was selected because it provides a recent observational snapshot close to the end of the NIRv-GPP record, and a fixed tundra mask was used to define a consistent spatial analysis domain. The MODIS land-cover data were derived from the MOD12Q1 Land Cover Science Data Product at a spatial resolution of 500 m (Friedl et al., 2010). This tundra distribution was used as a spatial mask to extract GPP, temperature, and precipitation data.

Monthly precipitation and 2-m air temperature data from 1982 to 2014 were sourced from the fifth generation European Center for Medium-Range Weather Forecasts climate reanalysis (ERA5) data set at 0.25° × 0.25° resolution (Hersbach et al., 2023). Monthly gross primary productivity (GPP) data set was derived from satellite near-infrared reflectance of vegetation (NIRv) from 1982 to 2014 with a spatial resolution of 0.05° × 0.05°. In addition, two GPP products, FLUXCOM-X GPP (Nelson et al., 2024) and Light Response Function (LRF)-based GPP (Tagesson et al., 2021), were used for robustness analyses; details are provided in Text S1 of Supporting Information S1.

We re-gridded temperature, precipitation, and GPP data to a common 0.5° × 0.5° grid and calculated growing-season means for each grid cell and year, with the growing season defined as months with monthly mean air temperature above 0°C (Karlsen et al., 2006; Liu et al., 2006). The Mann-Kendall test was then utilized to identify the greening and browning zones (see Section 2.3, Temporal trends analysis). Given that browning zones in the TP area could not be identified using the 0.5° × 0.5° resolution NIRv-GPP data, the original spatial resolution of

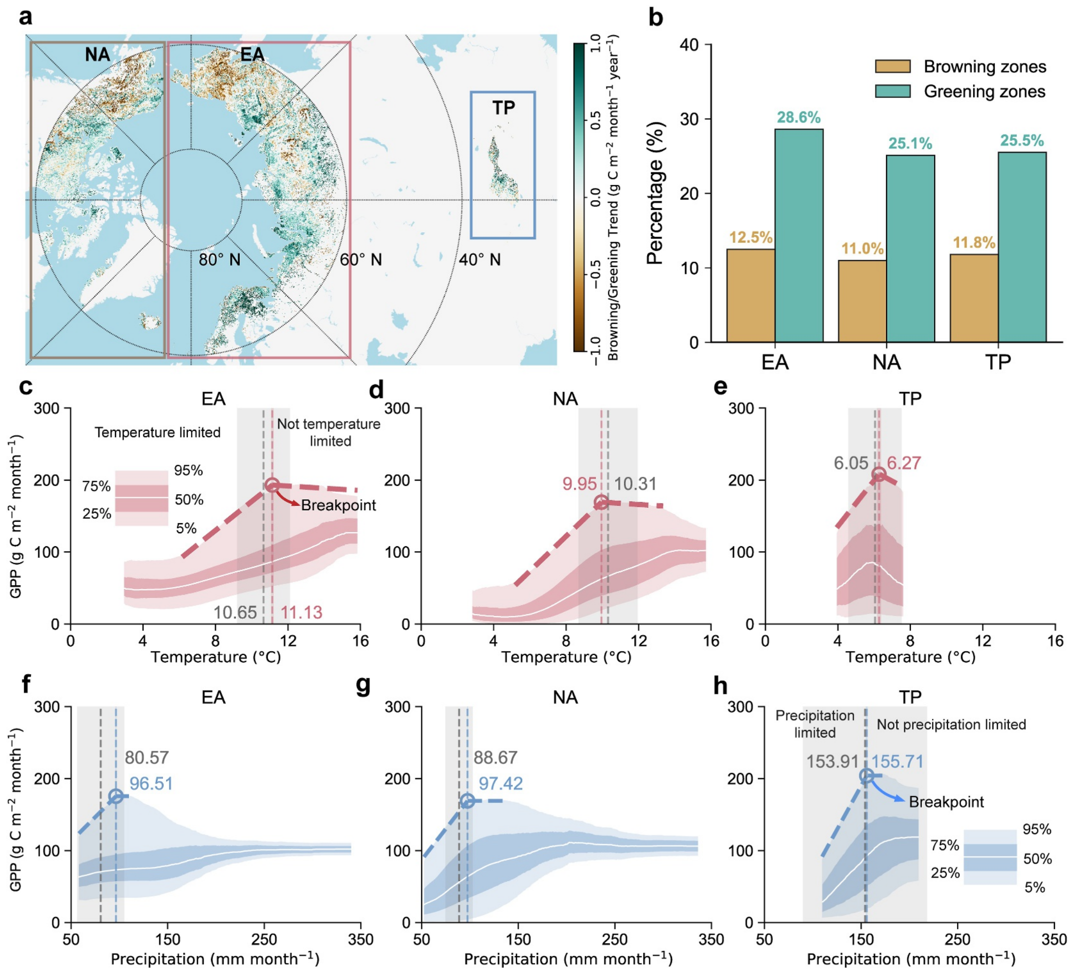

Figure 1. Relationships between temperature, precipitation, and NIRv-GPP for tundra in the Eurasian Arctic (EA), North American Arctic (NA), and the Tibetan Plateau (TP). (a) Spatial distribution of tundra grids with browning and greening trends between 1982 and 2014 in EA, NA, and the TP. (b) Proportions of grids showing significant browning and greening trends in the three regions. (c–e) Relationship between temperature and GPP in EA (c), NA (d), and the TP (e). (f–h) Relationship between precipitation and GPP in EA (f), NA (g), and the TP (h). GPP_{95} denotes the 95th percentile of GPP in each temperature or precipitation bin. Bold dashed lines indicate breakpoint regressions, and hollow circles denote estimated thresholds. Shading represents different GPP percentiles. Colored vertical dashed lines indicate the location of the thresholds derived from NIRV-GPP. Gray vertical dashed lines denote the mean thresholds derived from 14 ESMs, and the left and right borders of the gray vertical rectangles represent the mean of the 14 ESMs minus/plus one ensemble standard deviation. X_T and X_P for each model during 1982–2014 are provided in Figures S8–S13 in Supporting Information S1.

the NIRv-GPP data set was retained to differentiate between browning and greening zones when analyzing the historical period's threshold changes.

2.2. Coupled Model Intercomparison Project Phase 6 (CMIP6)

We used monthly outputs from 14 CMIP6 ESMs (Table S1 in Supporting Information S1). Monthly GPP was obtained directly from the CMIP6 output variable gpp, and near-surface air temperature (tas) and precipitation (pr) were taken from the same model, experiment, and realization. The gpp variable represents time-varying GPP simulated within each ESM. Because not all CMIP6 ESMs provide monthly gpp for both historical and SSP scenario simulations, we selected models with available monthly gpp, tas, and pr required for the threshold analysis. CMIP6 simulations include historical simulations (typically 1850–2014) and Shared Socioeconomic Pathway (SSP) scenario simulations (typically 2015–2100). We focused on SSP1–2.6, SSP2–4.5, and SSP5–8.5, which represent low-, intermediate-, and high-emission pathways. To maintain consistency across models, we used the first realization from each model, denoted as r1i1p1f1, following previous studies (Anav et al., 2013; Park & Jeong, 2021). Detailed information regarding the CMIP6 framework can be found in Eyring et al. (2016).

2.3. Temporal Trends Analysis

The Mann–Kendall test was employed to identify greening and browning zones, as well as trends in temperature and precipitation thresholds (Kendall, 1975; Mann, 1945). Considering the temporal coverage of the NIRv-GPP product and the CMIP6 historical/SSP framework, we analyzed historical trends for 1982–2014 and SSP scenario trends for 2015–2100. Specifically, grid cells with significant ($p < 0.05$) increasing NIRv-GPP trends during 1982–2014 were classified as greening zones, whereas those with significant decreasing trends were classified as browning zones. Linear regression was used to quantify the slopes of greening/browning trends and temperature/precipitation threshold changes.

2.4. Breakpoint Regression

GPP values were grouped into temperature or precipitation bins for each region and period. For each bin, we calculated the 95th percentile of GPP, denoted as GPP_{95}, to represent the high-productivity response under a given temperature or precipitation condition while reducing the influence of other environmental constraints such as cloudiness and drought. Breakpoint regression was then applied to GPP_{95} following previous studies (Donohue et al., 2013; Keenan & Riley, 2018; Ukkola et al., 2016). The breakpoint, where the GPP–temperature or GPP–precipitation relationship plateaus or shifts direction, was identified as the temperature or precipitation threshold beyond which GPP was no longer dominantly limited by that factor. Because breakpoint regression was applied to pooled regional samples, these thresholds characterize regional climate–GPP relationships rather than how a given ecosystem responds through time to climate change. Threshold uncertainty was estimated using 100 bootstrap resamples. The mean of the 100 fitted breakpoints was taken as the final threshold estimate, and the standard deviation across the 100 breakpoints was used to quantify its uncertainty (Keenan & Riley, 2018). Detailed information on the breakpoint regression implementation and uncertainty assessment is provided in Texts S3 and S4 of Supporting Information S1.

2.5. Proportion of Climate-Limited Range

To compare temperature and precipitation limitations between browning and greening zones, we calculated the fraction of each climate range over which GPP remained constrained. This fraction was defined as the difference between the threshold and the corresponding minimum growing-season value, divided by the full growing-season range of temperature or precipitation. Values close to 1 indicate limitation across most of the range, whereas values close to 0 indicate limitation over only a narrow range.

3. Results

3.1. Historical Trends in Temperature and Precipitation Thresholds

We used breakpoint regression to identify temperature thresholds (X_T) and precipitation thresholds (X_P) that limit GPP in tundra ecosystems in the Arctic and TP during 1982–2014, applied to both GPP derived from NIRv observations and CMIP6 ESM-simulated GPP. In tundra ecosystems of EA, NA and the TP, the X_T values derived from the NIRv-GPP data set were 11.13 ± 0.07°C, 9.95 ± 0.01°C, and 6.27 ± 0.12°C, respectively, while the X_P values were 96.51 ± 0.48 mm month^{-1} 97.42 ± 0.38 mm month^{-1}, and 155.71 ± 0.94 mm month^{-1}, respectively (Figure 1). The differences between the X_T derived from the NIRv-GPP data and the ensemble mean X_T derived from simulated GPP were marginal, ranging from 0.24°C to 0.48°C, while the differences in X_P ranged from 1.80 mm month^{-1} to 15.93 mm month^{-1}. Notably, these ESMs exhibit substantial differences in their representation of temperature acclimation, nitrogen cycle, and dynamic vegetation processes (Table S1 in Supporting Information S1). Accordingly, the temperature and precipitation thresholds derived from GPP simulations across different ESMs (Figure 1 and Figures S8–S13 in Supporting Information S1) also show pronounced variations—particularly for X_P over the TP. Compared with the TP, our results show that the Arctic tundra had higher X_T during 1982–2014, whereas the TP tundra exhibited higher X_P. This regional contrast was also reproduced by FLUXCOM-X GPP and LRF-based GPP (Text S3 and Figures S3, S4 in Supporting Information S1). These differences align with observed regional climate characteristics, with the Arctic showing warmer but drier growing seasons than the TP (Figure S15 in Supporting Information S1.

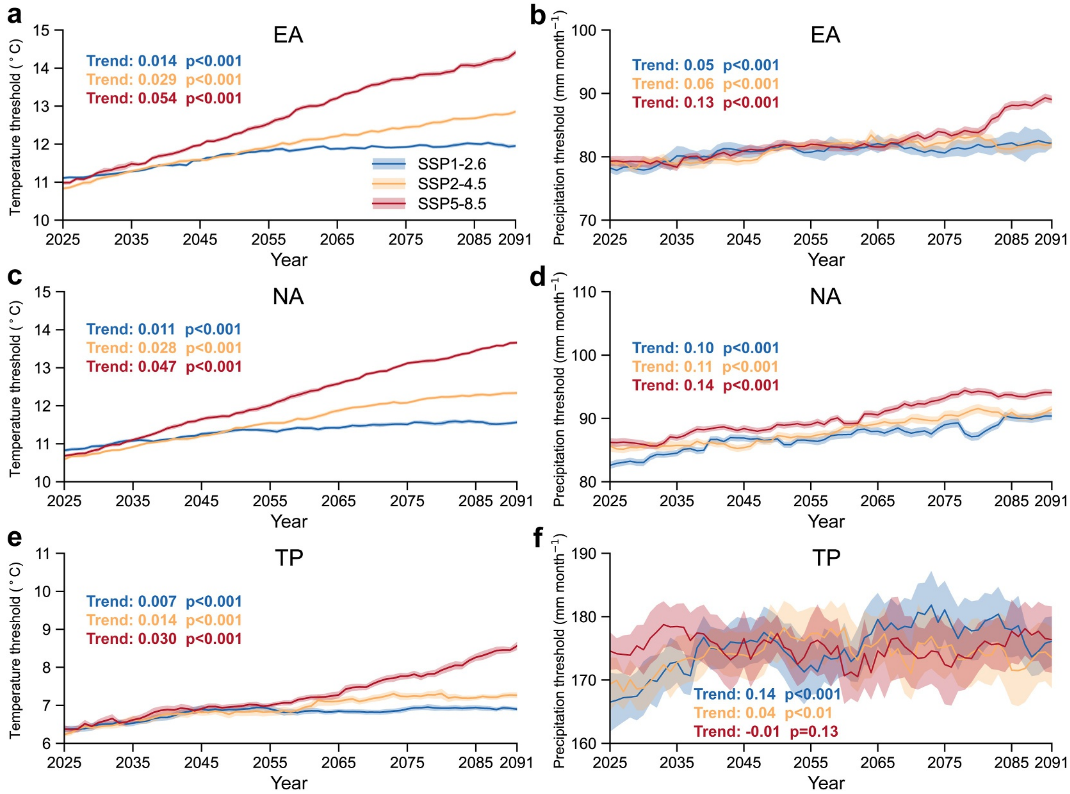

Figure 2. Projected trends of temperature thresholds and precipitation thresholds. (a, c, e) Projected trends of temperature thresholds (X_T) for EA, NA and the TP from 2015 to 2100. (b, d, f) Projected trends of precipitation thresholds (X_P) for EA, NA, and the TP. Thresholds were estimated independently for each ESM and each SSP scenario using 20-year running windows; the *x*-axis represents the rounded midpoint year of each window, for example, 2025 corresponds to 2015–2034. Colored lines represent the multi-model ensemble means for each SSP scenario, and shaded areas represent ±1 inter-model standard deviation across the 14 ESMs.

During 1982–2014, significant greening was more extensive than browning across EA, NA, and the TP, accounting for 25.1%–28.6% and 11.0%–12.5% of tundra grid cells, respectively (Figures 1a and 1b). Historical threshold trends in greening and browning zones are shown in Figure S14 of Supporting Information S1; overall, X_T increased in both zone types, whereas X_P generally decreased, except in TP greening zones.

3.2. Projected Trends in Temperature and Precipitation Thresholds

Based on projections from 14 CMIP6 ESMs for 2015–2100, we extracted and analyzed trends in mean growing-season temperature and precipitation (Figure S16 in Supporting Information S1), as well as the corresponding X_T and X_P for tundra ecosystems in the Arctic and TP (Figure 2). The multi-model ensemble mean indicates an increasing trend in X_T for both the Arctic and TP from 2015 to 2100 (Figure S17 in Supporting Information S1), although 2 out of 14 models projected a slight decline in X_T (lower than 0.01°C yr^{-1}) under the SSP1–2.6 scenario. Under SSP2–4.5 and SSP5–8.5, all models projected increasing trends in X_T, with larger increases under higher-emission pathways. Across all SSP scenarios, EA exhibited the largest increase in X_T, followed closely by NA, with rates approximately 1.5–2 times higher than those in the TP.

Compared to X_T, projected X_P trends exhibit larger variability across SSP scenarios and ESMs (Figure 2 and Figure S17 in Supporting Information S1). For both EA and NA, the multi-model ensemble mean indicates an overall increasing trend in X_P, with larger increases under higher-emission pathways. For NA, the projected rates across the three scenarios range from 0.97 to 1.39 mm $month^{-1}$ $decade^{-1}$, slightly higher than those for EA (0.50–1.33 mm $month^{-1}$ $decade^{-1}$). Specifically, X_P in NA increases steadily across all three scenarios, whereas in EA, X_P rises sharply around 2080–2085 under SSP 5-8.5, resulting in a marked divergence from the other scenarios thereafter. By contrast, the TP shows a less consistent trajectory across SSP scenarios and ESMs, which

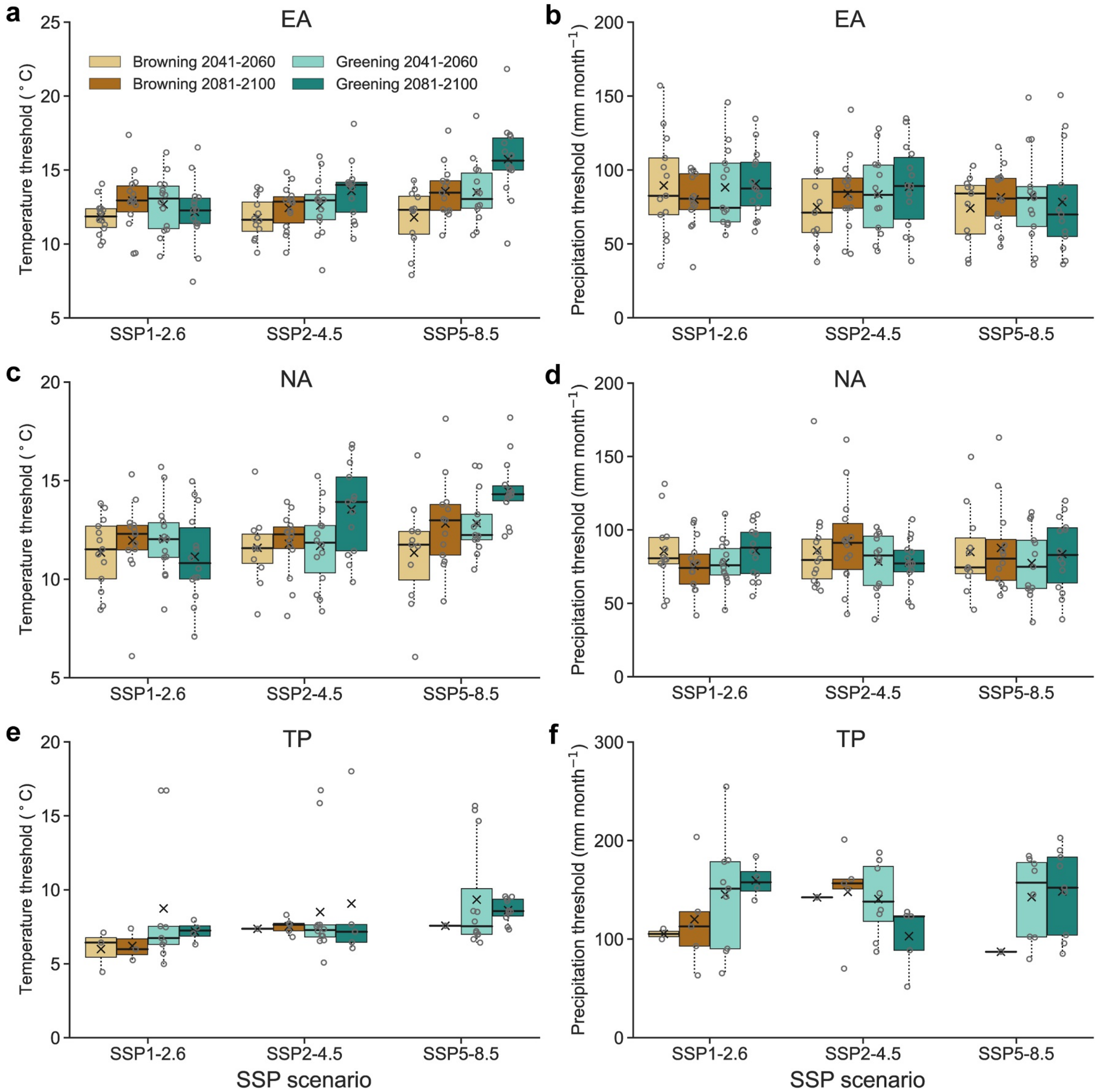

Figure 3. Temperature and precipitation thresholds for the browning and greening zones across two projected periods (2041–2060 and 2081–2100) under three SSP scenarios. (a, c, e) Temperature thresholds (X_T) for the browning and greening zones in EA, NA and the TP during 2041–2060 and 2081–2100 under SSP1–2.6, SSP2–4.5 and SSP5–8.5. (b, d, f) Similarly, precipitation thresholds (X_P) for the browning zones and greening zones in EA (b), NA (d) and the TP (f). Black hollow points indicate individual ESMs. Crosses and horizontal lines denote means and medians, respectively; boxes show the interquartile range (IQR), whiskers extend to 1.5 × IQR, and outliers are shown as points.

may reflect its smaller spatial extent, strong surface heterogeneity, and the larger inter-model spread in projected growing-season precipitation (Figure S16 in Supporting Information S1).

3.3. Projected Temperature and Precipitation Thresholds in Browning and Greening Zones

Building on the temporal trends of climate thresholds shown in Figure 2, we further analyzed projected X_T and X_P in the browning and greening zones across EA, NA, and the TP for the mid-21st-century (2041–2060) and late-21st-century (2081–2100) periods under different SSP scenarios. Due to the relatively coarse spatial resolution of CMIP6 ESM outputs, the number of identified greening and browning area pixels in the TP is limited, especially for browning areas. X_T and X_P in the TP are therefore detected by only a few ESMs (Figure 3). In the Arctic, the multi-model ensemble consistently projects increase in X_T for both browning and greening zones, with larger increases under higher-emission pathways. X_T in greening zones generally exceeds that in browning zones, except in 2081–2100 under SSP1–2.6. In the TP, higher X_T also tends to occur under high-emission scenarios and in greening zones. In contrast, projected X_P shows substantial overlap in its distributions across SSP scenarios, with no clear separation between browning and greening zones in EA, NA, and the TP.

The proportion of climate-limited ranges for browning and greening zones in EA and NA is shown in Figure S18 of Supporting Information S1. Most models project a larger precipitation-constrained fraction in browning zones than in greening zones, including 8 of 11 models in EA and nine of 12 in NA. Conversely, 8 of 13 models in EA and eight of 12 in NA project a larger temperature-constrained fraction in greening zones than in browning zones. These results suggest that by the end of this century, the GPP of Arctic tundra ecosystems in greening zones will be more strongly limited by temperature, whereas GPP in browning zones will be more strongly limited by precipitation.

4. Discussion

The temperature threshold for photosynthesis is a crucial parameter for understanding the relationship between climate and carbon exchange by terrestrial ecosystems. However, directly observed relationships between climate and tundra ecosystem CO_2 exchange are lacking. Our NIRv-GPP-derived X_T values in EA, NA, and the TP tundra were 11.13 ± 0.07°C, 9.95 ± 0.01°C, and 6.27 ± 0.12°C, respectively. These values are comparable to, but lower than previous findings (Yi et al., 2010), which reported that the sensitivity of net ecosystem exchange to mean annual temperature breaks down at approximately 16°C, beyond which no further increase in CO_2 uptake with temperature was observed. It should be noted that their findings were derived from a wide range of ecosystems (Yi et al., 2010), while the temperature sensitivity of vegetation productivity varies substantially across biomes. Ecosystem productivity generally exhibits lower optimal temperatures (T_{opt}), especially in TP grasslands (Huang et al., 2019), and a recent TP-focused study reported a regional mean T_{opt} of 9.32 ± 3.15°C for TP grasslands (Yin et al., 2026). Moreover, previous studies have shown that optimal temperatures are positively correlated with local mean annual temperatures (Chen et al., 2021; Niu et al., 2012). This pattern is consistent with our results of X_T across EA, NA, and the TP, implying a long-term adaptation of vegetation to climatic conditions (Kumarathunge et al., 2019).

Plants can adjust their physiological responses to temporal changes in ambient temperature, a response commonly known as thermal acclimation (Way & Yamori, 2014). In this study, we found increasing trends in X_T across EA, NA, and the TP during 1982–2014, with rates of 0.019, 0.013, and 0.009°C yr^{-1}, respectively. These trends are consistent with photosynthetic thermal acclimation. Here, X_T represents an apparent breakpoint in regional climate–GPP relationships, rather than a physiological optimum temperature. They are also broadly consistent with reported NIRv-derived global increases in T_{opt} over the past four decades (Fang et al., 2024; Wang et al., 2024), estimated as 0.017°C yr^{-1} and 0.03°C yr^{-1}, respectively. The most pronounced increase in X_T was observed in the Arctic, likely reflecting pronounced regional warming (Rantanen et al., 2022) and strong thermal acclimation capacity (Wang et al., 2024). Under SSP2–4.5, the multi-model ensemble projects the largest X_T increase during 2015–2100 in EA (0.029°C yr^{-1}), followed by NA (0.028°C yr^{-1}) and the TP (0.017°C yr^{-1}). These projected rates are also comparable to the estimated global increase rate in T_{opt} (0.027°C yr^{-1}) under the same scenario (Fang et al., 2024). Although X_T is projected to increase continuously, growing-season mean temperatures in these regions are expected to remain below X_T by 2100 (Figure S19 in Supporting Information S1), suggesting that GPP in these regions will continue to be limited by temperature during the growing season. However, maximum monthly growing-season temperatures have already exceeded X_T in the Arctic, and are projected to exceed X_T in the TP by the mid-21st century (Figure S19 in Supporting Information S1). These findings indicate a gradually weakening temperature limitation on GPP in both the Arctic and TP tundra ecosystems.

Across EA, NA, and the TP, regions with higher precipitation (e.g., the TP) also exhibit higher X_P, paralleling the temperature pattern and indicating a dependency of tundra vegetation photosynthesis on local precipitation conditions. This finding is consistent with previous studies (Ma et al., 2024; Zhang et al., 2021), highlighting the strong influence of water availability on photosynthesis in Arctic and TP vegetation, despite temperature often being considered the dominant factor. Under the SSP scenarios (SSP1–2.6, SSP2–4.5, and SSP5–8.5), multi-model ensemble projections show that X_P follows an overall increasing trend with fluctuations in both the Arctic and TP, and remains above the corresponding mean growing-season precipitation, indicating continued precipitation limitation on tundra photosynthesis. Although elevated CO_2 can enhance plant water-use efficiency, warming- and greening-enhanced evapotranspiration may offset this benefit and sustain future water limitation where precipitation is insufficient (Piao et al., 2020; Yang et al., 2023). Projected changes in X_P over the TP should be interpreted in terms of effective water availability rather than precipitation amount alone. TP vegetation dynamics are strongly linked to precipitation and monsoon variability (Li et al., 2020), while soil water content regulates GPP responses to environmental drivers, especially VPD, across TP alpine ecosystems (Zhang et al., 2024). Monsoon-driven precipitation variability, complex topography, soil water storage, and warming-enhanced evaporative demand therefore jointly regulate plant-available water, so increasing precipitation does not necessarily translate into uniform relief of water limitation. The differences between greening and browning zones further suggest contrasting dominant constraints: greening zones are projected to be more temperature-limited, whereas browning zones are more vulnerable to water limitation under compound soil and atmospheric dryness, consistent with recent evidence linking permafrost-region browning to concurrent soil moisture decline and rising VPD (Wu et al., 2026).

Based on the understanding of photosynthetic responses to rising temperatures, a representation scheme for photosynthetic temperature acclimation has been proposed (Kattge & Knorr, 2007) and implemented in many ESMs, including those used in this study (CMCC-CM2-SR5, CMCC-ESM2, NorESM2-MM, and IPSL-CM6A-LR, see Table S1 in Supporting Information S1). This scheme allows the peaked Arrhenius function to shift with growth temperature, leading to a higher temperature optimum under warmer conditions (Lombardozzi et al., 2015). This is consistent with our finding that the GPP temperature threshold of tundra ecosystems in the Arctic and TP increases with regional warming. Notably, these ESMs incorporating temperature acclimation generally project greater increases in temperature thresholds compared to those without such representation (Figure S17 in Supporting Information S1). Nevertheless, increasing X_T in models without explicit thermal acclimation is also plausible because X_T is inferred from regional climate–GPP relationships. Projected increases in precipitation over the Arctic and TP (Figure S16 in Supporting Information S1) may alleviate water limitation, allowing GPP to increase across a broader temperature range and thereby shifting apparent X_T upward. Recent studies have also revealed vegetation acclimation to soil moisture (Peng et al., 2024) and vapor pressure deficit (Abadie et al., 2025; Grossiord et al., 2017). However, the ESMs used in this study do not yet account for such water-related acclimation mechanisms, which may influence the robustness of our model-based projections, particularly for X_P. In addition, these models differ substantially in their representations of processes such as nitrogen and phosphorus cycling and dynamic vegetation, which are highly influential on terrestrial biogeochemistry and biophysics (Spafford & MacDougall, 2021).

Tundra ecosystems in both the TP and Arctic develop under harsh environmental conditions characterized by low mean annual temperature, limited precipitation, shallow and nutrient-poor soils, and a short growing season (S. Liu et al., 2018; Walker et al., 2005). These extreme conditions and unique ecosystem characteristics make field measurements and accurate ESM representation challenging (Henry et al., 2022). Constrained by limited availability of reliable observations and model simulations, meteorological data sets such as ERA5 are likely to carry considerable uncertainties in these regions (Jiao et al., 2021; Pernov et al., 2024). Similarly, sparse vegetation cover, together with the prevalence of seasonal snow and surface water may weaken the linkage between NIRv and GPP, rendering NIRv-based GPP estimates subject to substantial uncertainties (Nelson et al., 2022; Zeng et al., 2021). Considering the vulnerability of TP and Arctic tundra ecosystems to rapid climate change (Kuang & Jiao, 2016; Moon et al., 2024), it is essential to strengthen systematic observations and improve the representation of key variables such as climate drivers and vegetation physiological processes. This will advance our understanding of tundra ecosystem responses and feedbacks to ongoing climate change.

5. Conclusions

In summary, we examined how GPP-limiting temperature and precipitation thresholds in Arctic and TP tundra ecosystems have changed and are projected to change from 1982 to 2100, using observational data and CMIP6 simulations from 14 ESMs. We found that temperature thresholds are higher in the Arctic than in the TP, whereas precipitation thresholds are lower, reflecting adaptation of tundra vegetation to local climatic conditions. Over recent decades, temperature thresholds in both regions have increased and are projected to continue rising by 2100, while remaining above the mean growing-season temperature. This pattern is consistent with thermal acclimation of photosynthesis and suggests that temperature will continue to limit GPP in Arctic and TP tundra. In contrast, precipitation thresholds in the Arctic show significant upward trends, whereas those in the TP exhibit substantial temporal variability, likely reflecting the TP's complex precipitation regimes. By 2100, precipitation limitation is projected to exert a stronger influence in browning zones, whereas temperature limitation is expected to be more pronounced in greening zones. These findings provide insight into divergent climatic constraints on tundra ecosystems and can help improve predictions of carbon–climate feedbacks in the Arctic and TP.

Conflict of Interest

The authors declare no conflicts of interest relevant to this study.

Availability Statement

The ERA5 reanalysis dataset is available from the Copernicus Climate Change Service Climate Data Store at https://doi.org/10.24381/cds.f17050d7 (Hersbach et al., 2023). The MOD12Q1 Land Cover Type product is available from the NASA Land Processes Distributed Active Archive Center at http://doi.org/10.5067/MODIS/MCD12Q1.006 (Friedl & Sulla-Menashe, 2019). The NIRv-GPP dataset is available at https://doi.org/10.6084/m9.figshare.12981977 (Wang et al., 2020). The LRF-based GPP dataset is available at https://doi.org/10.17894/ucph.b2d7ebfb-c69c-4c97-bee7-562edde5ce66 (Tagesson et al., 2021). The FLUXCOM-X-BASE GPP dataset is available from the ICOS Carbon Portal at https://doi.org/10.18160/5NZG-JMJE (Nelson et al., 2023). CMIP6 Earth System Model outputs are available through Earth System Grid Federation (ESGF) portals, such as https://aims2.llnl.gov/search/cmip6/ (last accessed: 17 March 2024).

Acknowledgments
M.W. is supported by the National Key Research and Development Program of China (2024YFF0810900, 2023YFB3907402), the National Natural Science Foundation of China (42371486, 42111530184), the Fundamental Research Funds for the Central Universities (2026300415), and the Research Funds for the Frontiers Science Center for Critical Earth Material Cycling, Nanjing University (020914380115). H.W.C. received support from the Swedish Foundation for International Cooperation in Research and Higher Education (CH2020-8799). We thank Shengnan Zhu from Nanjing University for her contributions to data collection, processing, and analysis at the early stage of preparation. We acknowledge CMIP6 modeling groups for making their model outputs available.

References

Abadie, C., Maignan, F., Bacour, C., & Peylin, P. (2025). Evidence for vegetation acclimation to atmospheric dryness during European droughts from a land surface model. *Global Biogeochemical Cycles*, *39*(7), e2024GB008362. https://doi.org/10.1029/2024GB008362

Anav, A., Friedlingstein, P., Kidston, M., Bopp, L., Ciais, P., Cox, P., et al. (2013). Evaluating the land and Ocean components of the global carbon cycle in the CMIP5 Earth system models. *Journal of Climate*, *26*(18), 6801–6843. https://doi.org/10.1175/jcli-d-12-00417.1

Berner, L. T., Massey, R., Jantz, P., Forbes, B. C., Macias-Fauria, M., Myers-Smith, I., et al. (2020). Summer warming explains widespread but not uniform greening in the Arctic tundra biome. *Nature Communications*, *11*(1), 4621. https://doi.org/10.1038/s41467-020-18479-5

Bintanja, R., & Selten, F. M. (2014). Future increases in Arctic precipitation linked to local evaporation and sea-ice retreat. *Nature*, *509*(7501), 479–482. https://doi.org/10.1038/nature13259

Blunden, J., & Arndt, D. S. (2020). State of the Climate in 2019. *Bulletin of the American Meteorological Society*, *101*(8), S1–S429. https://journals.ametsoc.org/view/journals/bams/101/8/2020BAMSStateoftheClimate.xml

Chen, A., Huang, L., Liu, Q., & Piao, S. (2021). Optimal temperature of vegetation productivity and its linkage with climate and elevation on the Tibetan Plateau. *Global Change Biology*, *27*(9), 1942–1951. https://doi.org/10.1111/gcb.15542

Donohue, R. J., Roderick, M. L., McVicar, T. R., & Farquhar, G. D. (2013). Impact of CO2 fertilization on maximum foliage cover across the globe's warm, arid environments. *Geophysical Research Letters*, *40*(12), 3031–3035. https://doi.org/10.1002/grl.50563

Epstein, H. E., Raynolds, M. K., Walker, D. A., Bhatt, U. S., Tucker, C. J., & Pinzon, J. E. (2012). Dynamics of aboveground phytomass of the circumpolar Arctic tundra during the past three decades. *Environmental Research Letters*, *7*(1), 015506. https://doi.org/10.1088/1748-9326/7/1/015506

Eyring, V., Bony, S., Meehl, G. A., Senior, C. A., Stevens, B., Stouffer, R. J., & Taylor, K. E. (2016). Overview of the Coupled Model Intercomparison Project Phase 6 (CMIP6) experimental design and organization. *Geoscientific Model Development*, *9*(5), 1937–1958. https://doi.org/10.5194/gmd-9-1937-2016

Fang, Z., Zhang, W., Wang, L., Schurgers, G., Ciais, P., Peñuelas, J., et al. (2024). Global increase in the optimal temperature for the productivity of terrestrial ecosystems. *Communications Earth and Environment*, *5*(1), 466. https://doi.org/10.1038/s43247-024-01636-9

Friedl, M., & Sulla-Menashe, D. (2019). MCD12Q1 MODIS/Terra+Aqua land cover type yearly L3 global 500m SIN grid V006 [Dataset]. *NASA LP DAAC*. https://doi.org/10.5067/MODIS/MCD12Q1.006

Friedl, M. A., Sulla-Menashe, D., Tan, B., Schneider, A., Ramankutty, N., Sibley, A., & Huang, X. (2010). MODIS Collection 5 global land cover: Algorithm refinements and characterization of new datasets. *Remote Sensing of Environment*, *114*(1), 168–182. https://doi.org/10.1016/j.rse.2009.08.016

Goetz, S. J., Bunn, A. G., Fiske, G. J., & Houghton, R. A. (2005). Satellite-observed photosynthetic trends across boreal North America associated with climate and fire disturbance. *Proceedings of the National Academy of Sciences*, *102*(38), 13521–13525. https://doi.org/10.1073/pnas.0506179102

Grossiord, C., Sevanto, S., Borrego, I., Chan, A. M., Collins, A. D., Dickman, L. T., et al. (2017). Tree water dynamics in a drying and warming world. *Plant, Cell and Environment*, *40*(9), 1861–1873. https://doi.org/10.1111/pce.12991

Henry, G. H. R., Hollister, R. D., Klanderud, K., Björk, R. G., Bjorkman, A. D., Elphinstone, C., et al. (2022). The International Tundra Experiment (ITEX): 30 years of research on tundra ecosystems. *Arctic Science*, *8*(3), 550–571. https://doi.org/10.1139/as-2022-0041

Hersbach, H., Bell, B., Berrisford, P., Biavati, G., Horányi, A., Muñoz Sabater, J., et al. (2023). ERA5 monthly averaged data on single levels from 1940 to present [Dataset]. *Copernicus Climate Change Service (C3S) Climate Data Store (CDS)*. https://doi.org/10.24381/cds.f17050d7

Huang, M., Piao, S., Ciais, P., Peñuelas, J., Wang, X., Keenan, T. F., et al. (2019). Air temperature optima of vegetation productivity across global biomes. *Nature Ecology and Evolution*, *3*(5), 772–779. https://doi.org/10.1038/s41559-019-0838-x

Huxman, T. E., Smith, M. D., Fay, P. A., Knapp, A. K., Shaw, M. R., Loik, M. E., et al. (2004). Convergence across biomes to a common rain-use efficiency. *Nature*, *429*(6992), 651–654. https://doi.org/10.1038/nature02561

Jiao, D., Xu, N., Yang, F., & Xu, K. (2021). Evaluation of spatial-temporal variation performance of ERA5 precipitation data in China. *Scientific Reports*, *11*(1), 17956. https://doi.org/10.1038/s41598-021-97432-y

Karlsen, S. R., Elvebakk, A., Høgda, K. A., & Johansen, B. (2006). Satellite-based mapping of the growing season and bioclimatic zones in Fennoscandia. *Global Ecology and Biogeography*, *15*(4), 416–430. https://doi.org/10.1111/j.1466-822X.2006.00234.x

Kattge, J., & Knorr, W. (2007). Temperature acclimation in a biochemical model of photosynthesis: A reanalysis of data from 36 species. *Plant, Cell and Environment*, *30*(9), 1176–1190. https://doi.org/10.1111/j.1365-3040.2007.01690.x

Kattsov, V. M., Walsh, J. E., Chapman, W. L., Govorkova, V. A., Pavlova, T. V., & Zhang, X. (2007). Simulation and projection of Arctic freshwater budget components by the IPCC AR4 global climate models. *Journal of Hydrometeorology*, *8*(3), 571–589. https://doi.org/10.1175/jhm575.1

Keenan, T. F., & Riley, W. J. (2018). Greening of the land surface in the world's cold regions consistent with recent warming. *Nature Climate Change*, *8*(9), 825–828. https://doi.org/10.1038/s41558-018-0258-y

Kendall, M. G. (1975). *Rank correlation methods* (4th, 2d impression ed.). Griffin.

Kuang, X., & Jiao, J. J. (2016). Review on climate change on the Tibetan Plateau during the last half century. *Journal of Geophysical Research: Atmospheres*, *121*(8), 3979–4007. https://doi.org/10.1002/2015JD024728

Kumarathunge, D. P., Medlyn, B. E., Drake, J. E., Tjoelker, M. G., Aspinwall, M. J., Battaglia, M., et al. (2019). Acclimation and adaptation components of the temperature dependence of plant photosynthesis at the global scale. *New Phytologist*, *222*(2), 768–784. https://doi.org/10.1111/nph.15668

Li, P., Hu, Z., & Liu, Y. (2020). Shift in the trend of browning in Southwestern Tibetan Plateau in the past two decades. *Agricultural and Forest Meteorology*, *287*, 107950. https://doi.org/10.1016/j.agrformet.2020.107950

Liu, S., Zamanian, K., Schleuss, P.-M., Zarebanadkouki, M., & Kuzyakov, Y. (2018). Degradation of Tibetan grasslands: Consequences for carbon and nutrient cycles. *Agriculture Ecosystems and Environment*, *252*, 93–104. https://doi.org/10.1016/j.agee.2017.10.011

Liu, X., Yin, Z.-Y., Shao, X., & Qin, N. (2006). Temporal trends and variability of daily maximum and minimum, extreme temperature events, and growing season length over the eastern and central Tibetan Plateau during 1961–2003. *Journal of Geophysical Research*, *111*(D19). https://doi.org/10.1029/2005JD006915

Liu, Z., Ballantyne, A. P., Poulter, B., Anderegg, W. R. L., Li, W., Bastos, A., & Ciais, P. (2018). Precipitation thresholds regulate net carbon exchange at the continental scale. *Nature Communications*, *9*(1), 3596. https://doi.org/10.1038/s41467-018-05948-1

Lombardozzi, D. L., Bonan, G. B., Smith, N. G., Dukes, J. S., & Fisher, R. A. (2015). Temperature acclimation of photosynthesis and respiration: A key uncertainty in the carbon cycle-climate feedback. *Geophysical Research Letters*, *42*(20), 8624–8631. https://doi.org/10.1002/2015GL065934

Loranty, M. M., & Goetz, S. J. (2012). Shrub expansion and climate feedbacks in Arctic tundra. *Environmental Research Letters*, *7*(1), 011005. https://doi.org/10.1088/1748-9326/7/1/011005

Ma, D., Wu, X., Yin, G., Li, Z., Wang, J., Tang, R., et al. (2024). Detection, mapping, and interpretation of the main drivers of the Arctic GPP change from 2001 to 2019. *Climate Dynamics*, *62*(1), 723–738. https://doi.org/10.1007/s00382-023-06935-z

Mann, H. B. (1945). Nonparametric tests against trend. *Econometrica*, *13*(3), 245–259. https://doi.org/10.2307/1907187

Margesin, R. (2008). *Permafrost soils* (Vol. 16). Springer Science and Business Media.

Maricle, B. R., & Adler, P. B. (2011). Effects of precipitation on photosynthesis and water potential in Andropogon gerardii and Schizachyrium scoparium in a southern mixed grass prairie. *Environmental and Experimental Botany*, *72*(2), 223–231. https://doi.org/10.1016/j.envexpbot.2011.03.011

Maurer, G. E., Hallmark, A. J., Brown, R. F., Sala, O. E., & Collins, S. L. (2020). Sensitivity of primary production to precipitation across the United States. *Ecology Letters*, *23*(3), 527–536. https://doi.org/10.1111/ele.13455

Moon, T. A., Druckenmiller, M. L., & Thoman, R. L. (2024). NOAA Arctic Report Card 2024: Executive Summary. Technical Report./view/noaa/66870.

Nelson, J. A., Walther, S., Gans, F., Kraft, B., Weber, U., Novick, K., et al. (2024). X-BASE: The first terrestrial carbon and water flux products from an extended data-driven scaling framework, FLUXCOM-X. *Biogeosciences*, *21*(22), 5079–5115. https://doi.org/10.5194/bg-21-5079-2024

Nelson, J. A., Walther, S., Jung, M., Gans, F., Kraft, B., Weber, U., et al. (2023). FLUXCOM-X-BASE. https://meta.icos-cp.eu/collections/zfwf1Ak2I7OlziGDTX8Xl6_T

Nelson, P. R., Maguire, A. J., Pierrat, Z., Orcutt, E. L., Yang, D., Serbin, S., et al. (2022). Remote sensing of Tundra ecosystems using high spectral resolution reflectance: Opportunities and challenges. *Journal of Geophysical Research: Biogeosciences*, *127*(2), e2021JG006697. https://doi.org/10.1029/2021JG006697

Niu, S., Luo, Y., Fei, S., Yuan, W., Schimel, D., Law, B. E., et al. (2012). Thermal optimality of net ecosystem exchange of carbon dioxide and underlying mechanisms. *New Phytologist*, *194*(3), 775–783. https://doi.org/10.1111/j.1469-8137.2012.04095.x

Park, H., & Jeong, S. (2021). Leaf area index in Earth system models: How the key variable of vegetation seasonality works in climate projections. *Environmental Research Letters*, *16*(3), 034027. https://doi.org/10.1088/1748-9326/abe2cf

Peng, J., Tang, J., Xie, S., Wang, Y., Liao, J., Chen, C., et al. (2024). Evidence for the acclimation of ecosystem photosynthesis to soil moisture. *Nature Communications*, *15*(1), 9795. https://doi.org/10.1038/s41467-024-54156-7

Pernov, J. B., Gros-Daillon, J., & Schmale, J. (2024). Comparison of selected surface level ERA5 variables against in-situ observations in the continental Arctic. *Quarterly Journal of the Royal Meteorological Society*, *150*(761), 2123–2146. https://doi.org/10.1002/qj.4700

Piao, S., Wang, X., Park, T., Chen, C., Lian, X., He, Y., et al. (2020). Characteristics, drivers and feedbacks of global greening. *Nature Reviews Earth and Environment*, *1*(1), 14–27. https://doi.org/10.1038/s43017-019-0001-x

Rantanen, M., Karpechko, A. Y., Lipponen, A., Nordling, K., Hyvärinen, O., Ruosteenoja, K., et al. (2022). The Arctic has warmed nearly four times faster than the globe since 1979. *Communications Earth and Environment*, *3*(1), 168. https://doi.org/10.1038/s43247-022-00498-3

Spafford, L., & MacDougall, A. H. (2021). Validation of terrestrial biogeochemistry in CMIP6 Earth system models: A review. *Geoscientific Model Development*, *14*(9), 5863–5889. https://doi.org/10.5194/gmd-14-5863-2021

Tagesson, T., Tian, F., Schurgers, G., Horion, S., Scholes, R., Ahlström, A., et al. (2021). A physiology-based Earth observation model indicates stagnation in the global gross primary production during recent decades. *Global Change Biology*, *27*(4), 836–854. https://doi.org/10.1111/gcb.15424

Ukkola, A. M., Prentice, I. C., Keenan, T. F., van Dijk, A. I. J. M., Viney, N. R., Myneni, R. B., & Bi, J. (2016). Reduced streamflow in water-stressed climates consistent with CO2 effects on vegetation. *Nature Climate Change*, *6*(1), 75–78. https://doi.org/10.1038/nclimate2831

Walker, D. A., Raynolds, M. K., Daniëls, F. J. A., Einarsson, E., Elvebakk, A., Gould, W. A., et al. (2005). The Circumpolar Arctic vegetation map. *Journal of Vegetation Science*, *16*(3), 267–282. https://doi.org/10.1111/j.1654-1103.2005.tb02365.x

Wang, S., Zhang, Y., & Ju, W. (2020). Long-term (1982–2018) global gross primary production dataset based on NIRv [Dataset]. *Figshare*. https://doi.org/10.6084/m9.figshare.12981977

Wang, X., Pang, G., & Yang, M. (2018). Precipitation over the Tibetan Plateau during recent decades: A review based on observations and simulations. *International Journal of Climatology*, *38*(3), 1116–1131. https://doi.org/10.1002/joc.5246

Wang, Y., Sarmah, S., Singha, M., Chen, W., Ge, Y., Liang, L. L., et al. (2024). Increasing Optimum temperature of vegetation activity over the past four decades. *Earth's Future*, *12*(10), e2024EF004489. https://doi.org/10.1029/2024EF004489

Way, D. A., & Yamori, W. (2014). Thermal acclimation of photosynthesis: On the importance of adjusting our definitions and accounting for thermal acclimation of respiration. *Photosynthesis Research*, *119*(1), 89–100. https://doi.org/10.1007/s11120-013-9873-7

Wu, M., Sonnentag, O., Lara, M. J., Ran, Y., Chen, H. W., Zhang, W., et al. (2026). Vegetation browning patterns under compound soil and atmospheric dryness in northern permafrost ecosystems. *Nature Communications*, *17*(1), 8194. https://doi.org/10.1038/s41467-026-75131-4

Xu, L., Myneni, R. B., Chapin Iii, F. S., Callaghan, T. V., Pinzon, J. E., Tucker, C. J., et al. (2013). Temperature and vegetation seasonality diminishment over northern lands. *Nature Climate Change*, *3*(6), 581–586. https://doi.org/10.1038/nclimate1836

Xu, Z. X., Gong, T. L., & Li, J. Y. (2008). Decadal trend of climate in the Tibetan Plateau—Regional temperature and precipitation. *Hydrological Processes*, *22*(16), 3056–3065. https://doi.org/10.1002/hyp.6892

Yang, Y., Roderick, M. L., Guo, H., Miralles, D. G., Zhang, L., Fatichi, S., et al. (2023). Evapotranspiration on a greening Earth. *Nature Reviews Earth and Environment*, *4*(9), 626–641. https://doi.org/10.1038/s43017-023-00464-3

Yi, C., Ricciuto, D., Li, R., Wolbeck, J., Xu, X., Nilsson, M., et al. (2010). Climate control of terrestrial carbon exchange across biomes and continents. *Environmental Research Letters*, *5*(3), 034007. https://doi.org/10.1088/1748-9326/5/3/034007

Yin, G., Xie, J., Wang, Y., Chen, R., Yang, Y., Ma, D., et al. (2026). Incorporating thermal adaptation and acclimation improves light-use efficiency modeling for estimating gross primary production in Tibetan Plateau grasslands. *Global Change Biology*, *32*(5), e70911. https://doi.org/10.1111/gcb.70911

You, Q., Cai, Z., Pepin, N., Chen, D., Ahrens, B., Jiang, Z., et al. (2021). Warming amplification over the Arctic Pole and Third Pole: Trends, mechanisms and consequences. *Earth-Science Reviews*, *217*, 103625. https://doi.org/10.1016/j.earscirev.2021.103625

Zeng, Y., Hao, D., Badgley, G., Damm, A., Rascher, U., Ryu, Y., et al. (2021). Estimating near-infrared reflectance of vegetation from hyperspectral data. *Remote Sensing of Environment*, *267*, 112723. https://doi.org/10.1016/j.rse.2021.112723

Zhang, T., Shan, B., Xu, M., Zhao, G., Zheng, Z., Tang, Y., et al. (2024). Soil moisture alters the responses of alpine ecosystem productivity to environmental factors, especially VPD, on the Qinghai-Tibetan Plateau. *Science of the Total Environment*, *947*, 174518. https://doi.org/10.1016/j.scitotenv.2024.174518

Zhang, Y., Hu, Q., & Zou, F. (2021). Spatio-Temporal changes of vegetation net primary productivity and its driving factors on the Qinghai-Tibetan Plateau from 2001 to 2017. *Remote Sensing*, *13*(8), 1566. https://doi.org/10.3390/rs13081566

Zhong, L., Ma, Y., Salama, M. S., & Su, Z. (2010). Assessment of vegetation dynamics and their response to variations in precipitation and temperature in the Tibetan Plateau. *Climatic Change*, *103*(3), 519–535. https://doi.org/10.1007/s10584-009-9787-8

Zhu, Z., Piao, S., Myneni, R. B., Huang, M., Zeng, Z., Canadell, J. G., et al. (2016). Greening of the Earth and its drivers. *Nature Climate Change*, *6*(8), 791–795. https://doi.org/10.1038/nclimate3004

References From the Supporting Information

Wang, S., Zhang, Y., Ju, W., Qiu, B., & Zhang, Z. (2021). Tracking the seasonal and inter-annual variations of global gross primary production during last four decades using satellite near-infrared reflectance data. *Science of the Total Environment*, *755*, 142569. https://doi.org/10.1016/j.scitotenv.2020.142569

Zhang, Y., & Ye, A. (2021). Would the obtainable gross primary productivity (GPP) products stand up? A critical assessment of 45 global GPP products. *Science of the Total Environment*, *783*, 146965. https://doi.org/10.1016/j.scitotenv.2021.146965